Water SA 48(2) 187–198 / Apr 2022
https://doi.org/10.17159/wsa/2022.v48.i2.3903

Research paper

Adsorption and desorption studies of *Carica papaya* stem activated with zinc chloride for mining wastewater treatment

Ezekiel A Adetoro[1], Samson O Ojoawo[1] and AM Salman[2]

[1]*Department of Civil Engineering, Ladoke Akintola University of Technology, P.M.B. 4000, Ogbomoso, Nigeria*
[2]*Department of Civil and Environmental Engineering, Kwara State University, Malete, Nigeria*

The adsorption of eight selected potentially toxic metal ions from actual mining wastewater obtained from Igbeti, Nigeria, was established using activated carbon chemically prepared from *Carica papaya* stem with zinc chloride (CPSAC-$ZnCl_2$) as activating agent. Characterization of the prepared CPSAC-$ZnCl_2$ sample for surface morphology and functional groups was done by scanning electron microscopy (SEM) and Fourier transform infrared (FTIR) spectroscopy, respectively. An atomic absorption spectrophotometer (AAS) was utilized for characterization of the selected metals in the mining wastewater. Batch adsorption and desorption studies were conducted on removal of the metals from the sample using CPSAC-$ZnCl_2$. The data obtained were fitted to isotherm (Freundlich and Langmuir); kinetic (pseudo-second-order and intra-particle diffusion) and thermodynamic (standard enthalpy change – $\Delta H°$, entropy change – $\Delta S°$ and free energy change – $\Delta G°$) models. These were considered under two error functions (sum of absolute errors – SAE, coefficient of determination – R^2) of linear and non-linear regression analyses. The SEM micrograph revealed that the CPSAC-$ZnCl_2$ sample was 2.0–50.0 nm with FTIR spectra absorption peaks ranging from 746.2 to 3 987.0 cm^{-1}. The initial concentrations of selected metals in the wastewater varied from 5.7 to 756.5 mg/L. The adsorbent dosage, agitation rate, contact time, pH and temperature for optimum condition of CPSAC-$ZnCl_2$ were 0.6 g, 150.0 r/min, 60 min, pH of 7.0 and 30°C, respectively. The selected metals' adsorption onto CPSAC-$ZnCl_2$ followed Freundlich and Langmuir isotherm models pseudo-second-order kinetics with intra-particle diffusion mechanism. The $\Delta H°$, $\Delta S°$ and $\Delta G°$ for the processes were 134.5, 64.5 and 22 012.0 kJ/mol, respectively. The adsorbent achieved an adsorption efficiency of above 95.0%, and is thus recommended for industrial application in remediating potentially toxic metals from wastewater.

CORRESPONDENCE
Ezekiel A Adetoro

EMAIL
yemmieadyt@yahoo.com

DATES
Received: 21 April 2021
Accepted: 10 April 2022

KEYWORDS
error function
isotherms
kinetic
thermodynamic
toxic metals

COPYRIGHT
© The Author(s)
Published under a Creative Commons Attribution 4.0 International Licence (CC BY 4.0)

INTRODUCTION

Toxic metals as pollutants in wastewater impose serious health risks and environmental problems when discharged as industrial effluents. They are hazardous and non-biodegradable with a persistent nature (Smily and Sumithra, 2017), thus must be removed from industrial effluents before being discharged into water to avoid harm to ecosystems and humans (Alalwan, 2020).

There are methods available for remediation of potentially toxic metals from the environment, such as filtration, ion exchange and membrane separation, among others. These have shortcomings, such as high cost, disposal of sludge, being energy- and time-intensive, and with low productivity in the case of low concentrations of metals. The method of biosorption, which has the ability of complete sequestration of potentially toxic metals from wastewater (even at very low concentrations), using capable, efficient and inexpensive biomaterials, has been receiving increasing attention. Biosorption is an innovative and eco-friendly method, which has potential for regeneration and metal recovery through the desorption process, thereby enabling re-use and providing a solution to the problem of waste sludge (Smily and Sumithra, 2017; Czikkely et al., 2018, Aghalari et al., 2020).

The application of activated carbon (AC), which has effective functional groups and a large surface area, as an adsorbent in wastewater treatment is hindered by its high cost; hence, the need for alternative low-cost materials having a similar function to conventional AC (Acheampong and Ansa, 2017; Biswas et al., 2019). Agricultural biomaterials (as precursors), such as *Azadirachta indica* (neem) leaf, African spinach stalk (ASS), cocoa husk pod, coconut shell, guinea corn stem, maize cob, *Moringa oleifera* husk, pods and leaves, orange peel, tea dust, among others, have been used successfully in bioremediation of potentially toxic metals from wastewater (Table 1). *Carica papaya* stem (CPS), as an agricultural biomaterial, shares similar properties with some of the above-mentioned adsorbents (Table 2 provides a summary of the chemical properties of a range of biomaterials). Thus it was selected as a potential adsorbent for removal of metals from Igbeti marble mining wastewater.

This study investigated the use of CPS, an agricultural bio-resource that is very common in Third World nations like Nigeria, in addressing the environmental problems due to the presence of potentially toxic metals in mining wastewater through bioremediation. This aimed to derive a cost-effective, practical, reliable and accessible technique for wastewater treatment. This study will promote the adoption of a 'waste to wealth policy'.

There is little information available in literature on the use of *Carica papaya* stem activated carbon produced from zinc chloride activating agent (CPSAC-$ZnCl_2$) in treating wastewater such as mining wastewater (see Table 1). Thus, the focus of this study was on the adsorption and desorption

Table 1. Adsorption potential for some adsorbents for metal ion removal from wastewater

Adsorbent	Activating agents	Adsorbate	Metals removed	Adsorption process models	RE (%)	Error functions	References
Neem leaf powder	NaOH	Synthetic wastewater	Cu^{2+}	Freundlich and Langmuir	77.4	R^2 (linear regression)	Sulaiman and Garba (2014)
Coconut shell	NR	Synthetic wastewater	Cr (VI)	Freundlich, Langmuir, pseudo-first- order, ΔH, ΔG and ΔS	84.1	R^2 (linear regression)	Ayub and Korasgani (2014)
Carica papaya leaves	HNO_3	Synthetic wastewater	Pb^{2+}	Freundlich, Langmuir	NR	R^2 (linear regression)	Suyono et al., 2015
Used tea dust	H_3PO_4	Tannery wastewater	Cr^{3+}	NR	70	R^2 (linear regression)	Shalna and Yogamoorthi, 2015
Feldspar clay	*Carica papaya* seed	Synthetic wastewater	Cu^{2+} and Pb^{2+}	Langmuir, ΔH, ΔG and ΔS	92.5–94.8	R^2 (linear regression)	Sanusi et al., 2016
Activated charcoal – 250	NR	Foundry wastewater	Pb^{2+} and Cu^{2+}	Freundlich, pseudo-second-order	100.0	R^2 (linear regression)	Ojoawo and Udayakumar, 2016
CPS peel	NR	Synthetic wastewater	Pb^{2+} and Cr^{3+}	Freundlich, Langmuir, pseudo-second-order	47.4–68.8	R^2 (linear regression)	Ojoawo et al., 2016
Orange peel	HNO_3	Synthetic wastewater	Cd^{2+}	Freundlich, Langmuir, pseudo-second-order	89.6	R^2 (linear regression)	Emenike et al., 2016
Melon husk	H_2SO_4 and $NaHCO_3$	Synthetic wastewater	Cd^{2+}	Freundlich, pseudo-first-order	96.8	R^2 (linear regression)	Emenike et al., 2016
Chestnut shell	NaOH	Synthetic wastewater	Cd^{2+}	Freundlich, pseudo-second-order	98.3	R^2 (linear regression)	Emenike et al., 2016
Carica papaya peel	HNO_3, $C_2H_4O_2$, H_3PO_4, KOH, $CaCl_2$ and NaOH	Synthetic wastewater	Ammoniacal nitrogen	NR	31.6	R^2 (linear regression)	Musa et al., 2017
Rice husk	NR	Synthetic wastewater	Cu^{2+}, Cd^{2+}	Freundlich, Langmuir, pseudo-second-order	80–97.6	R^2 (linear regression)	El-Moselhy et al., 2017
CPS	$ZnCl_2$	Actual mining wastewater	Cu^{2+}, Mn^{2+}, Co^{3+}, Fe^{2+}, Zn^{2+}, Cd^{2+}, Pb^{2+}, Cr^{3+}	Freundlich, Langmuir, pseudo-second-order, intra-particle diffusion, ΔH, ΔG and ΔS	> 95.0	SAE and R^2 for both linear and non-linear regression	This study

NR – not reported

Table 2. Some chemical properties of some agricultural biomaterials (source: *Azadirachta indica* and used tea dust – Adetoro and Ojoawo (2020a), *Moringa oleifera* leaf – Bello et al. (2019) and *Carica papaya* – this study)

S/No.	Sample	Moisture (%)	Ash (%)	Fixed carbon (%)
1	*Carica papaya*	3.00	7.38	69.10
2	*Azadirachta indica*	3.10	4.48	82.25
3	*Moringa oleifera* leaf	8.08	12.71	69.41
4	Used tea dust	1.90	12.40	73.09

efficiencies of CPSAC-$ZnCl_2$ in removing selected metal ions from actual mining wastewater sourced from a marble mining site in Igbeti, south-western Nigeria. Batch adsorption and desorption experiments, fitting of adsorption process models (i.e. isotherms – Freundlich and Langmuir, kinetic – pseudo-second-order and intra-particle diffusion, and thermodynamics – $\Delta H°$, $\Delta S°$ and $\Delta G°$) and error functions (i.e. SAE and R^2 assessments of linear and non-linear regression analyses) were conducted.

METHODS

Preparation of adsorbent

Carica papaya stem (CPS) collected from Ladoke Akintola University of Technology Research Farm, Ogbomoso, Nigeria, was shredded and carefully washed with deionized water in order to get rid of impurities present in it. The washed CPS sample was oven-dried at 105°C for a day and then ground into powder. The CPS powder was poured into washed heating pots, placed in a muffle furnace (model number 5X1-1008 at 600°C) for an additional hour before being removed and allowed to cool. The carbonized sample was thoroughly washed with deionized water till it reached a pH of 7.0, oven-dried at 105°C for 2 h and then allowed to cool. This procedure was conducted in accordance with Bello et al. (2019).

The prepared carbonized CPS sample (50.0 g) was placed in a bottle and soaked with 0.1 M zinc chloride (i.e. activating agent – 500.0 mL), sieved after 24 h and thoroughly washed with deionized water till it reached a pH of 7.0, dried at 105°C, allowed to cool and kept in a desiccator (Bello et al., 2019).

Characterization of the prepared CPSAC-$ZnCl_2$ adsorbent

The CPSAC-$ZnCl_2$ was characterized by functional groups and surface morphology, using a scanning electron microscope (SEM) and Fourier transform infrared (FTIR) spectroscopic analyses.

FTIR spectroscopic analysis

The typical functional groups present on the adsorbent's surface (i.e. the chemistry of surface of the raw CPS and CPSAC-$ZnCl_2$)

were determined through FTIR spectroscopic analysis using Infrared Spectrophotometer (Buck Model 530). The spectra range required to capture the needed functional groups was estimated at 4 000.0 to 400.0 cm^{-1}. The dried sample (1 mg) and KBr (500.0 mg) (Merck, for spectroscopy) were blended in a transparent mortar and the resulting blend was subsequently pressed at 10 000.0 kg cm^{-2} for 15 min under vacuum. The FTIR spectra revealed the functional groups typical of the raw and CPSAC-$ZnCl_2$ adsorbent surfaces(after Bello et al., 2019).

SEM analysis

The surface morphological structure of the CPSAC-$ZnCl_2$ sample was assessed using a SEM (Model VPFESEM Supra 35VP) and images of 20 µm sizes with 500 x magnification (after Bello et al., 2019).

Determination of wastewater metal concentrations

A mining wastewater sample was collected from Igbeti marble mining site in south-western Nigeria. The mining wastewater and blank samples (10.0 mL each) were put into two different heating bottles (one for each) and nitric acid (HNO_3 – 15.0 mL) was gently mixed with the contents, covered, heated for 5.0 to 10.0 min, cooled, then filtered into a transparent flask using glass funnels and Whatman filter papers. The filtrates were increased to 100.0 mL with deionized water and put into transparent tightly corked bottles in preparation for the AAS reading. This procedure was conducted in accordance with ULM (2017).

The filtrates were then analysed for the concentrations of selected metal ions (i.e. Cu^{2+}, Mn^{2+}, Co^{3+}, Fe^{2+}, Zn^{2+}, Cd^{2+}, Pb^{2+} and Cr^{3+}) using AAS (Model no. PG 990). The results were converted to mg/L. This procedure was utilized for metal ions analyses of the mining wastewater prior to and after treatment with the adsorbent.

Batch adsorption experiments

The adsorption factors considered for the experiments were adsorbent dosage (i.e. 0.2, 0.4, 0.6, 0.8 and 1.0 g), agitation rate (i.e. 50.0, 100.0, 150.0, 200.0 and 250.0 r/min), contact time (i.e. 20.0, 40.0, 60.0, 80.0, 100.0 and 120.0 min), grain size (i.e. 0.08, 0.13, 0.25, 0.43, 1.00 and 2.00 mm), pH (i.e. 4.0, 6.0, 8.0 and 10.0) and temperature (i.e. 30.0, 40.0, 50.0, 60.0 and 70.0 °C). The mining wastewater sample (50 mL) was poured into a transparent flask and the different adsorbent dosages administered, agitated using J.P. Selecta orbital shaker (model number 3000974) at different agitation rates, contact time, grain size, pH and temperature, using one-factor-at-a-time (OFAT) analysis. The suspensions were filtered using glass funnels and Whatman filter papers. The selected metal ion concentrations present in the filtrates were then examined using AAS and analysed statistically. The adsorption capacity – q_e (mg/g) and removal efficiency – RE (%) were calculated using Eqs 1 and 2, respectively.

$$q_e = \frac{(C_o - C_e)V}{W} \quad (1)$$

$$RE = \frac{(C_o - C_e)}{C_o} \times 100\% \quad (2)$$

where V = solution volume (mL), W = amount of adsorbent (g), C_o and C_e = initial and equilibrium concentration of the solution (mg/L) (Adetoro and Ojoawo, 2020a).

Desorption experiments

Desorption experiments were carried out 6 times (at the end of each batch adsorption process) using modified methods of Al-Fakih (2015) and Smily and Sumithra (2017), in order to study the adsorbent's reusability and efficiency. The desorbing agent used was hydrochloric acid (HCl – 0.1 M) due to its efficiency and effectiveness as reported by Al-Fakih (2015) and others. The used adsorbent was always soaked in 15.0 mL of the desorbing agent for 2 h, before being centrifuged in an orbital centrifuge at 250.0 r/min for 20 min at room temperature (30°C), filtered, washed continuously inside BS Sieve 40 (i.e. 0.43 mm) with deionized water until pH of 6.9–7.0 was attained, oven-dried at 105°C, and allowed to cool for 2 h. The desorbed adsorbent was then used for another batch adsorption study. The desorption efficiency (DE) (%) was determined using Eq. 3:

$$DE = \frac{\text{Quantity of metal ion desorbed}}{\text{Quantity of metal ion adsorbed}} \times 100\% \quad (3)$$

Adsorption isotherms

Comparisons were made between the obtained batch adsorption data and two selected adsorption isotherms, Freundlich and Langmuir. Equations 4 and 5 were utilized for non-linear and linear analyses of the Freundlich isotherm, respectively. Langmuir isotherm suitability was established using Eqs 6 (non-linear), 7 (linear) and 8 (separation factor).

$$q_e = KC_e^{1/n} \quad (4)$$

$$\log q_e = \log K + \frac{1}{n}\log C_e \quad (5)$$

Irreversible, non-optimum and optimum adsorption processes were represented by $1/n = 0$, $1/n > 1$ and $0 < 1/n < 1$, respectively (after Bello et al., 2019; Adetoro and Ojoawo, 2020b).

$$q_e = \frac{q_m \cdot K \cdot C_e}{1 + K \cdot C_e} \quad (6)$$

$$\frac{C_e}{q_e} = \frac{1}{q_m \cdot K} + \frac{C_e}{q_m} \quad (7)$$

$$R_L = \frac{1}{(1 + K \cdot C_o)} \quad (8)$$

where K = Langmuir parameter for adsorption capacity and q_m = Langmuir parameter for adsorption energy. Non-optimum, linear, irreversible and optimum adsorption requires that $R_L > 1$, 1, 0 and $0 < R_L < 1$ respectively (Bello et al., 2019; Adetoro and Ojoawo, 2020b).

Adsorption kinetics

The batch adsorption data were compared with two selected adsorption kinetics models: pseudo-second-order and intra-particle diffusion. Equations 9 and 10 were used for linear and non-linear analyses of the pseudo-second-order kinetic model, while intra-particle diffusion analysis was carried out using Eq. 11 (after Bello et al., 2019; Adetoro and Ojoawo, 2020b).

$$q_t = \frac{K_2 \cdot t \cdot q_e^2}{K_2 \cdot t \cdot q_e + 1} \quad (9)$$

$$\frac{t}{q_t} = \frac{1}{K_2 \cdot q_e^2} + \frac{t}{q_e} \quad (10)$$

$$q_t = K_{diff}(t^{\frac{1}{2}}) + C \quad (11)$$

where K_2 = pseudo-second-order rate constant, q_t and q_e = adsorption capacity at time t and equilibrium respectively, K_{diff} is the intra-particle diffusion rate constant (mg/(g·min)) and C is the intercept (Bello et al., 2019; Adetoro and Ojoawo, 2020b).

Adsorption thermodynamics

The adsorption data were also assessed using three thermodynamic parameters: standard enthalpy variation ($\Delta H°$); standard entropy

variation ($\Delta S°$) and standard free energy variation ($\Delta G°$). $\Delta H°$ and $\Delta S°$ were determined using Eqs 12 and 13, respectively, while $\Delta G°$ was determined from Eq. 14. The system's chemical or physical nature was determined through Arrhenius equation (i.e. Eq. 15), while the magnitude of the activation energy (E_a) was established from the gradient of a plot of ln K_2 against $1/T$. When $5.0 \leq E_a \leq 40.0$ kJ/mol, this indicates physisorption and when $40.0 \leq E_a \leq 800.0$ kJ/mol, this indicates chemisorption (Bello et al., 2019; Adetoro and Ojoawo, 2020b).

$$\ln K = \frac{\Delta S^0}{\mathrm{R}} - \frac{\Delta H^0}{\mathrm{RT}} \quad (12)$$

K is derived from Eq. 22:

$$K = \frac{C_{ae}}{C_e} \quad (13)$$

$$\Delta G^0 = -\mathrm{RT} \cdot \ln K \quad (14)$$

$$\ln K = \ln A - \frac{E_a}{\mathrm{RT}} \quad (15)$$

where A = Arrhenius factor, E_a = Arrhenius activation energy of adsorption (kJ/mol) and C_{ae} is the equilibrium concentration adsorbed (mg / L).

Error functions

Two error functions, namely, sum of absolute errors (SAE) and coefficient of determination (R^2) were applied for linear and non-linear regression analyses of the selected adsorption isotherms and kinetic models. Equations 16 and 17 were utilized for SAE and R^2 error functions respectively (Adetoro and Ojoawo, 2020b).

$$\mathrm{SAE} = \sum_{i=1}^{n} (q_e(\mathrm{expt}) - q_e(\mathrm{calc}))_i \quad (16)$$

$$R^2 = 1 - \frac{\sum_{i=1}^{n} (q_e(\mathrm{calc}) - q_e^{\mathrm{mean}}(\mathrm{expt}))_i^2}{(\sum_{i=1}^{n} (q_e(\mathrm{calc}) - q_e^{\mathrm{mean}}(\mathrm{expt}))_i^2 + \sum_{i=1}^{n} (q_e(\mathrm{calc}) - q_e(\mathrm{expt}))_i^2)} \quad (17)$$

where q_e(calc), q_e(expt) and q_e^{mean}(expt) are the adsorption capacities established from the modelled, experimental and mean experimental results.

RESULTS AND DISCUSSION

Characterization of the produced CPSAC-$ZnCl_2$ adsorbent

Figure 1 shows the raw CPS and CPSAC adsorbent produced.

FTIR analysis

Figure 2 shows the FTIR ranges for raw CPS and CPSAC-$ZnCl_2$. The raw CPS FTIR spectrum was compared with that of CPSAC-$ZnCl_2$ to indicate shifts in IR peaks. The FTIR spectra showed that most peaks were shifted either downward or upward, while a few appeared or disappeared. The variation in the magnitude of peaks was due to chemical bonds formed in CPS functional groups, thus confirming the potential for adsorption of different pollutants by

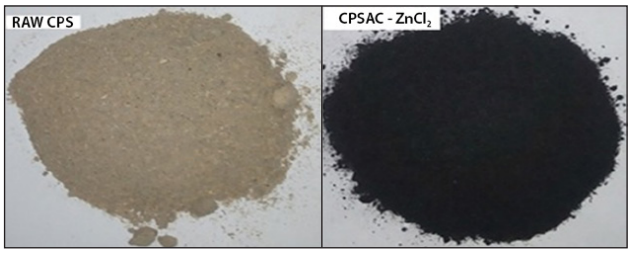

Figure 1. Adsorbents produced from *Carica papaya* stem (CPS)

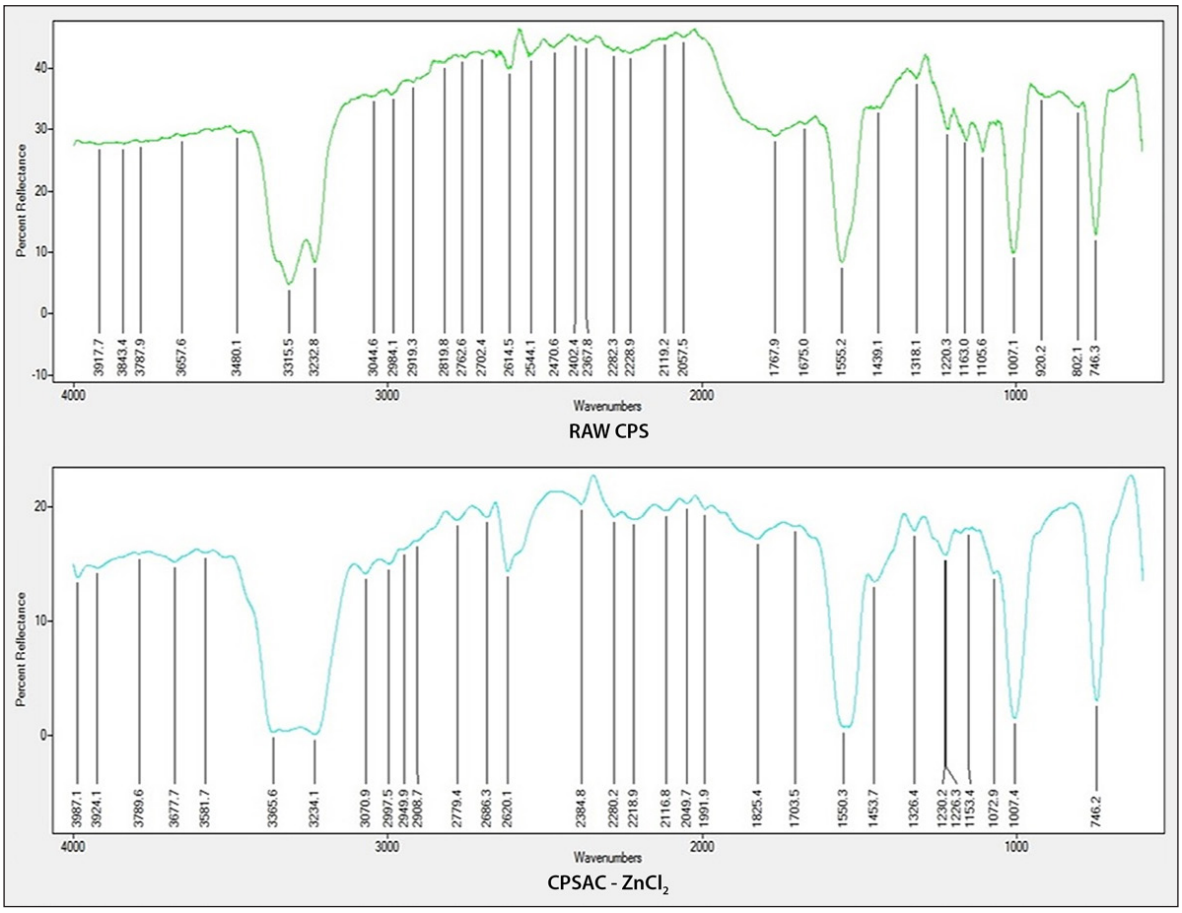

Figure 2. Surface chemistry – FTIR spectrum of raw CPS and CPSAC-$ZnCl_2$

CPS, with satisfactory removal efficiency likely, based on the FTIR. The FTIR spectroscopic analyses for both adsorbent revealed IR peaks ranging from 3 987.1 to 746.2 cm^{-1}, as shown in Fig. 3 and Table 3. The IR peaks observed in the raw CPS ranged from 3 917.7 to 746.3 cm^{-1} and the percentage reflectance ranged between 0.0 and 50.0 (Fig. 3). The C–O stretch bond that ranged from 1 220.3 to 1007.1 cm^{-1} and C–Br stretch bond at 746.3 cm^{-1} shifted downward, while the C–O stretch bond at 1 264.2 cm^{-1} and C–Cl stretch at 802.1 cm^{-1} appeared and disappeared, respectively, after activation. IR peaks of 3 987.1 to 746.2 cm^{-1} were observed for CPSAC-$ZnCl_2$, while the percentage reflectance ranged between 0 and 25 (Figure 2). The changes in the IR spectra between the raw CPS and CPSAC-$ZnCl_2$ are shown in Table 3. It was observed that the IR peaks of the O–H stretch bond at 3 787.9, 3 657.6, 3 315.5, 3 232.8, C=O stretch bond and N=H bend bond at 3 044.6, 2 984.1, 2 919.3, 2 762.6 and 2 614.5 cm^{-1} shifted upward, while that at 2 702.4 cm^{-1} shifted downward, after activation. C=O stretch and N=H bend bond types disappeared at 3 480.1, 2 819.8, 2 544.1, 2 470.6, 2 402.4 cm^{-1}, while O–H stretch bond at 3 581.7 cm^{-1}, C=O stretch bond and N=H bend bond at 2 908.7 cm^{-1} IR peaks appeared after activation. C≡C and C≡N stretch bond types at 2 282.3, 2 228.9 and 2 119.2 cm^{-1} shifted downward. The C=O stretch at 1 767.9 and 1 675.0 cm^{-1} shifted downward and disappeared, respectively.

Table 3. Changes in the IR spectra of the raw CPS and CPSAC-$ZnCl_2$

RAW CPS		CPSAC-$ZnCl_2$		Remarks
IR peak	**Functional group**	**IR peak**	**Functional group**	
		3 987.1		Appeared
3 917.7		3 924.1		Shifted upward
3 843.4				Disappeared
3 787.9	Alcohols, phenols and carboxylic acids	3 789.6	Alcohols, phenols and carboxylic acids	Shifted upward
3 657.6		3 677.7		Shifted upward
		3 581.7		Appeared
3 480.1	Amides			Disappeared
3 315.5	Aldehydes, amides, carboxylic acids, ketones and lactones	3 365.6	Alcohols, phenols and carboxylic acids	Shifted upward
3 232.8		3 234.1		Shifted upward
3 044.6		3 070.9	Aldehydes, amides, Carboxylic acids, ketones and lactones	Shifted upward
2 984.1		2 997.5		Shifted upward
2 919.3		2 949.9		Shifted upward
		2 908.7		Appeared
2 819.8	Aldehydes, amides, carboxylic acids, ketones and lactones			Disappeared
2 762.6		2 779.4	Aldehydes, amides, carboxylic acids, ketones and lactones	Shifted upward
2 702.4		2 686.3		Shifted downward
2 614.5		2 620.1		Shifted upward
2 544.1				Disappeared
2 470.6				Disappeared
2 402.4				Disappeared
2 367.8		2 384.8		Shifted upward
2 282.3	Alkynes and nitrites	2 280.2	Alkynes and nitrites	Shifted downward
2 228.9		2 218.9		Shifted downward
2 119.2		2 116.8		Shifted downward
2 057.5		2 049.7		Shifted downward
		1 991.9		Appeared
		1 825.4		Appeared
1 767.9	Aldehydes, carboxylic acids, ketones & lactones	1 703.5	Aldehydes, carboxylic acids, ketones & lactones	Shifted downward
1 675.0				Disappeared
1 555.2	Amides	1 550.3	Amides	Shifted downward
1 439.1		1 453.7	Amides	Shifted upward
1 318.1	Aromatic amines & primary or secondary OH	1 326.4	Aromatic amines & primary or secondary OH	Shifted upward
		1 230.2	Aldehydes, carboxylic acids, ketones & lactones	Appeared
1 220.3	Aldehydes, carboxylic acids, ketones & lactones	1 226.3		Shifted upward
1 163.0		1 153.4		Shifted downward
1 105.6		1 072.9		Shifted downward
1 007.1		1 007.4		Shifted upward
920.2				Disappeared
802.1	Amines			Disappeared
746.3	Esters	746.2	Esters	Shifted downward

The N=H bend at 1 555.2 and 1 439.1 cm^{-1} shifted downward and upward, respectively, while C–N stretch bond at 1 318.1 cm^{-1} and C–O stretch bond at 1 220.3 and 1 007.1 cm^{-1} shifted upward. Those at 1 163.0, 1 105.6 cm^{-1} and C–Br stretch bond at 746.3 cm^{-1} shifted downward, while C–O stretch appeared at 1 230.2 cm^{-1} and C–Cl stretch disappeared at 802.1 cm^{-1} after activation, as explained by Coates (2014). The changes in FTIR spectra confirmed the effects of activation on raw CPS. The shifts in the spectra portrayed that CPSAC-$ZnCl_2$ would be useful in the removal of metals from mining wastewater. Thus, activation plays an important role in enhancing the functional groups on the adsorbent. Generally, the presence of functional groups, which include alcohols, aldehydes, amines, carboxylic, esters, lactones, ketones, phenols and ether groups, in the adsorbent gave it the ability to bind metal ions by donation of an electron pair from these groups to form complexes with the metal ions in solution, as explained by Bello et al. (2019). Thus, there is the potential for CPSAC-$ZnCl_2$ adsorbent to remove metals ions from wastewater.

SEM analysis

The surface morphology of CPSAC-$ZnCl_2$ is shown in Fig. 3. The surfaces were rough, uneven and many pores had formed, due to the modification of the material using the activating agent. A pore structure with several rough cavities distributed over the adsorbent's surface resulted from the breakdown of lignocellulose material at high temperature. The evaporation of volatile compounds usually results in materials with well-developed pores. The increase in the rate of reaction during the activation process resulted in carbon 'burn off', and developed good pores on the precursor. There was an increase in the porosity of the material and creation of new pores as a result of carbon loss via CO and CO_2 forms. The physiochemical treatments thus resulted in porous materials, as expressed by Adetoro and Ojoawo (2020b). The surface of the CPSAC has many large pores in a honeycomb shape, indicating the effectiveness of the activating agent (i.e. $ZnCl_2$) in creating heterogeneous and well-developed pores on the precursor's surface, leading to CPSAC with a large porous surface structure. These pores provided suitable surfaces for metals to be trapped and adsorbed.

Mining wastewater metal concentrations

The concentrations of selected metal ions in the mining wastewater, prior to and after treatment, are given in Table 4. None of the selected metal concentrations met the WHO (2011) standards for drinking water quality prior to treatment. This indicated that the marble mining site's surrounding environment is likely to be contaminated by the mining wastewater. After treatment, there were still Co, Fe and Pb ions in the mining wastewater at quantities higher than the WHO (2011) limits, despite significant remediation, while the remaining metal ions (Cu^{2+}, Mn^{2+}, Zn^{2+}, $Cd^{2+}$and Cr^{3+}) were totally removed (i.e. not detected – ND) by CPSAC-$ZnCl_2$. However, raw CPS succeeded in remediating only two potentially toxic metals (i.e. Zn^{2+} and Cd^{2+}), while the remaining metal ions (Cu^{2+}, Mn^{2+}, Fe^{2+}, Co^{3+}, $Pb^{2+}$and Cr^{3+}) were reduced, but to levels that were still higher than the WHO (2011) required standards.

The increase in the number of potentially toxic metals removed (i.e. from 2 to 6) when treated with CPSAC-$ZnCl_2$ confirmed the effects of activation on raw CPS. Thus, activation plays an important role in enhancing the functional groups on the adsorbent and enabling the ability of the CPS adsorbent to remove metal ions from the mining wastewater. The activation of raw CPS with $ZnCl_2$ improves its removal efficiency (RE) and adsorption capacity (q_e).

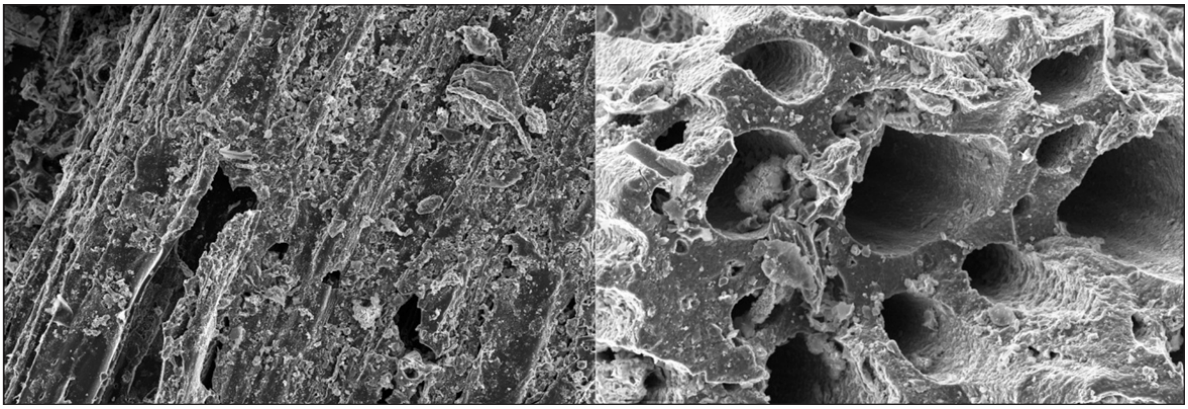

Figure 3. Surface morphology of CPSAC-$ZnCl_2$ using SEM (magnification: x 500)

Table 4. Concentrations of metal ions in mining wastewater

Metal	Concentration (mg/L)			
	Prior to treatment	After treatment		WHO (2011) standards
	Mining wastewater	CPSAC-$ZnCl_2$	Raw CPS	
Cadmium	37.40	ND	ND	0.00
Chromium	66.20	ND	0.44	0.05
Cobalt	9.60	0.03	0.93	-
Copper	31.40	ND	1.65	1.00
Iron	756.50	1.57	5.67	0.30
Manganese	5.70	ND	0.50	0.20
Lead	45.80	1.02	2.00	0.01
Zinc	94.10	ND	ND	3.00

ND – not detected

Results of batch adsorption experiments

Effect of adsorbent dosage

Percentage removal (RE) by different CPSAC-$ZnCl_2$ and raw CPS dosages are shown in Fig. 4, with Cr^{3+} having the lowest removal efficiency. It was also observed that percentage removal increases with the increasing dosage from 0.2 to 0.6 g, where optimum removal was attained and then remained constant from 0.6 to 1.0 g for all the metals studied. The optimum RE for Mn^{2+}, Co^{3+}, Fe^{2+}, Pb^{2+} and Cr^{3+} at 0.6 g adsorbent dosage were 100, 99.68, 99.83, 98.74 and 100%, respectively, for the CPSAC-$ZnCl_2$ adsorbent.

There was an increase in RE for the selected metals with increasing raw CPS dosage from 0.2 to 1.0 g. The optimum RE for Mn^{2+}, Co^{3+}, Fe^{2+}, Pb^{2+} and Cr^{3+} was achieved at 1.0 g, with maximum RE of 91.2, 90.3, 99.3, 95.6 and 99.3, respectively. The adsorption capacities for all the potentially toxic metals decreased with increase in adsorbent dosage. This is attributed to the decrease in total surface area of the adsorbent and increase in diffusion path length, which resulted in aggregation of adsorbent particles. The aggregation becomes increasingly important as the weight of the adsorbent increases, as explained by Sanusi et al. (2016).

Effect of agitation rate

The effect of agitation rate on metal removal by CPSAC-$ZnCl_2$ and raw CPS is shown in Fig. 5. The RE for all the metals increased as the agitation rate increased, up until 150.0 r/min, after which it remained the same for CPSAC-$ZnCl_2$ adsorbent; while RE continued to improve up until 200.0 r/min for raw CPS. The optimum agitation rate for the treatment was thus attained at 150.0 and 200.0 r/min for CPSAC-$ZnCl_2$ and raw CPS, respectively. The lowest RE was recorded for Co^{3+} and Pb^{2+} by CPSAC-$ZnCl_2$ and raw CPS, respectively.

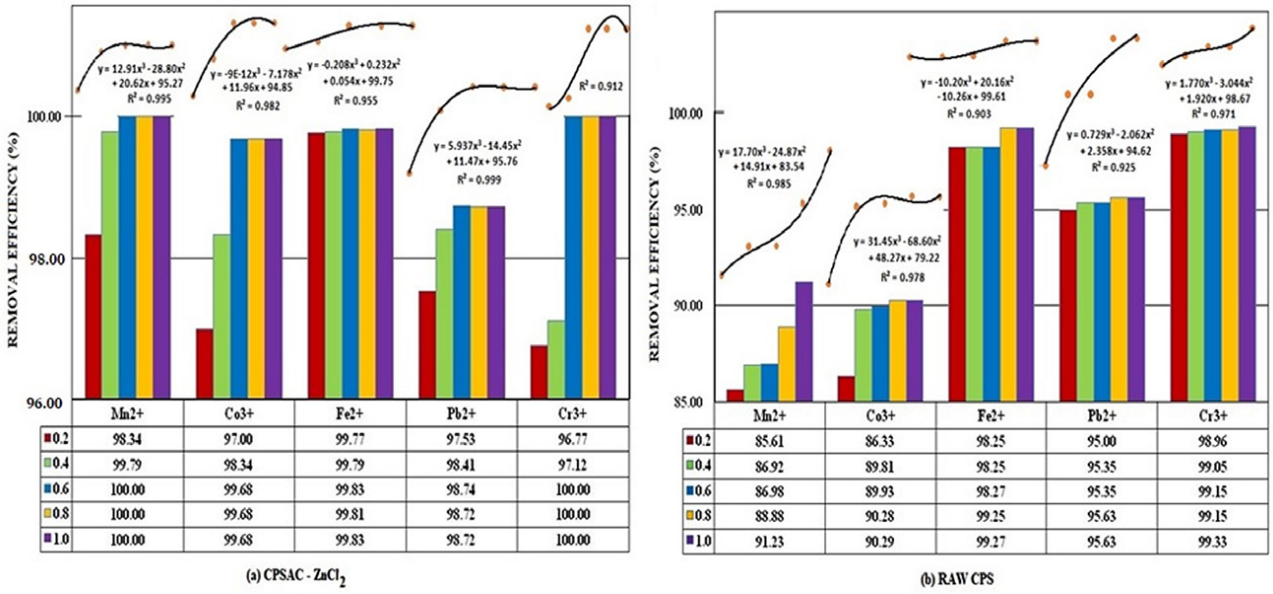

Figure 4. Metal removal efficiency trends with different CPSAC-$ZnCl_2$ and raw CPS dosages (agitation rate of 150 r/min, contact time of 60 min, grain size of <2.0 mm, and temperature of 30°C were constant during the experiment)

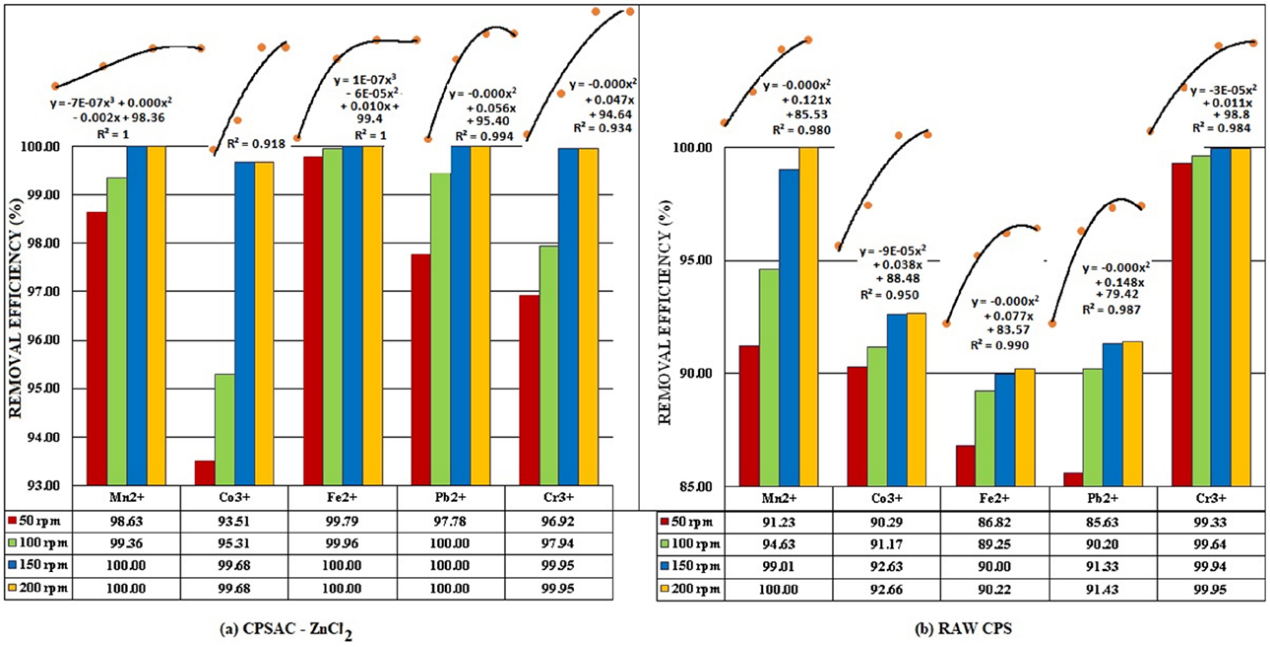

Figure 5. Metal removal efficiency trend with agitation rate (adsorbent dosage of 0.6 g (CPSAC-$ZnCl_2$) and 1.0 g (raw CPS), contact time of 60 min, grain size of <2.0 mm, and temperature of 30°C were constant during the experiment)

Effect of contact time

Effect of contact time on metal removal by CPSAC-$ZnCl_2$ and raw CPS is shown in Fig. 6. It was observed that removal efficiencies for the metals increased from 20–60 min then remained the same from 60–120 min for CPSAC-$ZnCl_2$. Thus optimum RE was achieved at 60 min and contact time variation of 60–120 min has no noticeable effects during the treatment. The peak of percentage removal for Mn^{2+}, Co^{3+}, Fe^{2+}, Pb^{2+} and Cr^{3+} stood at 100, 99.68, 99.83, 97.79 and 100%, with Pb^{2+} recorded the lowest RE.

For metals removal by raw CPS, RE increased with increase in contact time throughout the process. The peak of percentage removal for Mn^{2+}, Co^{3+}, Fe^{2+}, Pb^{2+} and Cr^{3+} stood at 92.1, 97.4, 89.4, 86.1 and 89.5%, respectively. The optimum contact time for the adsorption process was 120 min. The results show that Cr^{3+} was removed to the least extent by the treatment. There were sharp increases in the adsorption of the metal ions on the CPSAC-$ZnCl_2$ within the first 20–40 min of the process; the slower adsorption after this may be due to the blocking of some pores on the adsorbent surface by anionic constituents of the *Carica papaya* stem. This is because the pore sizes on the powdered *Carica papaya* stem's surface are larger than the sizes of the metal ions. Thus, there is a possibility of the negative ions at the surface of the adsorbent diffusing into and blocking the pores after modification. Consequently, the metal ions may not be able to diffuse further into the pores; hence, the increase in the overall rate of adsorption is reduced, as explained by Sanusi et al. (2016).

Effect of grain size

Effects of changes in grain sizes of CPSAC-$ZnCl_2$ and raw CPS on metal removal from mining wastewater are shown in Fig. 7. All the potentially toxic metals showed decreases in percentage removal as the grain size increased from 0.08 to 2.00 mm, for both

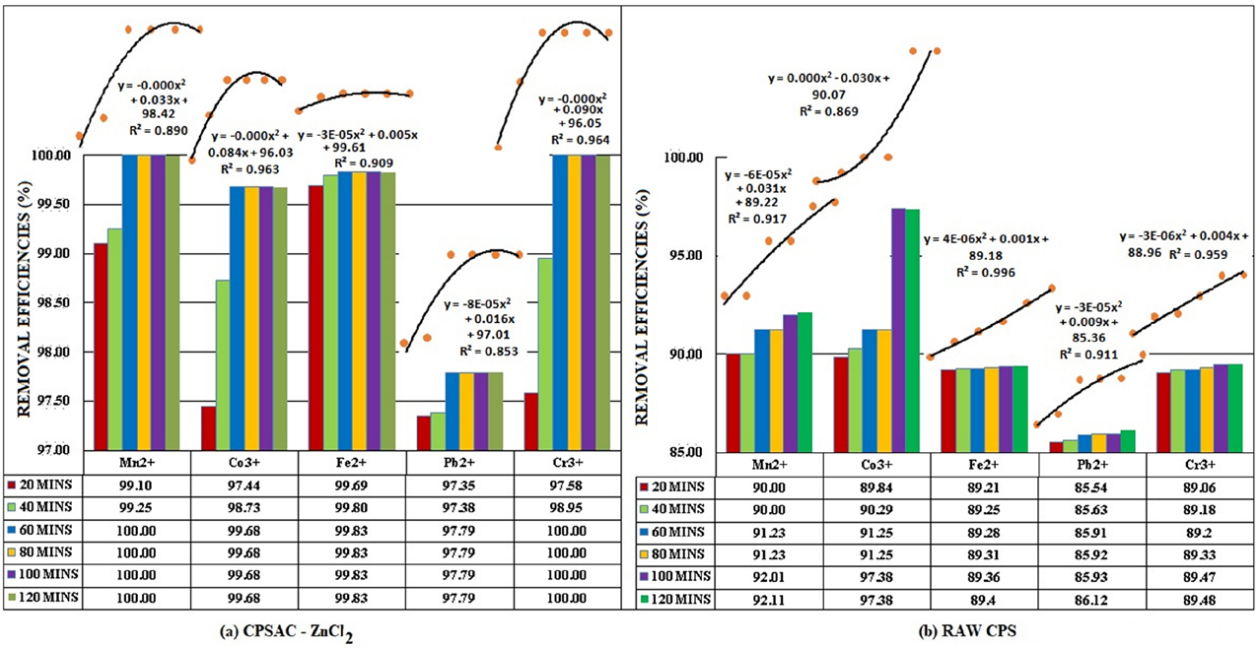

Figure 6. Metal removal efficiency trend with contact time (adsorbent dosage of 0.6 g (CPSAC-$ZnCl_2$) and 1.0 g (raw CPS), agitation rate of 150 r/min, grain size of <2.0 mm, and temperature of 30°C were constant during the experiment)

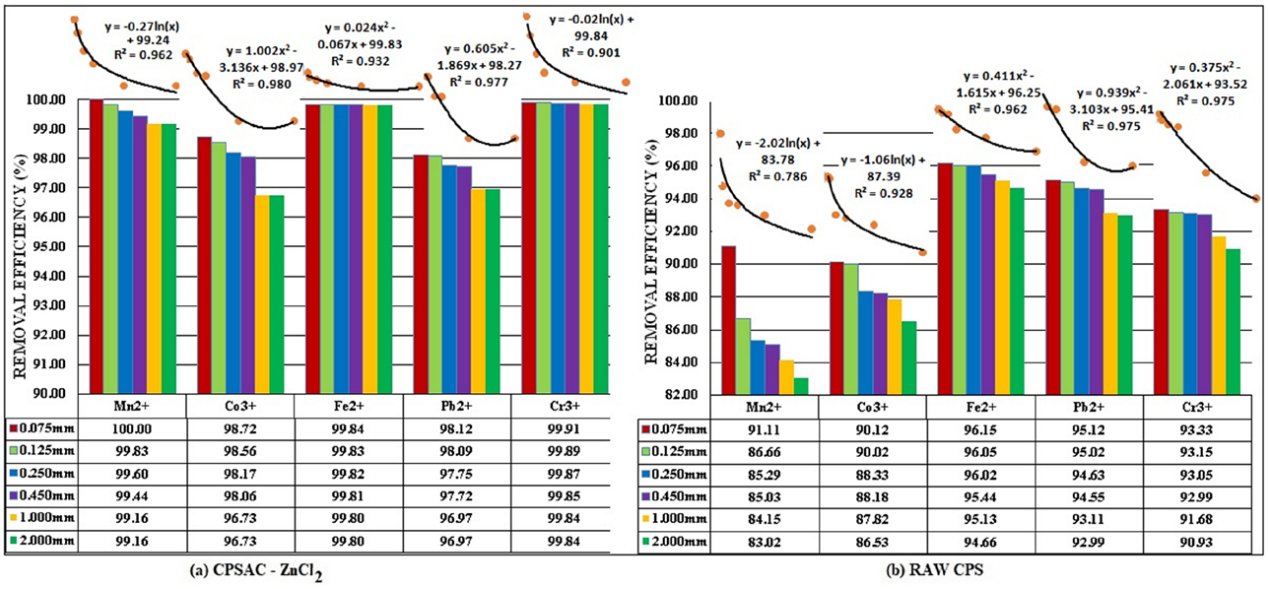

Figure 7. Metal removal efficiency trend with grain size (adsorbent dosage of 0.6 g (CPSAC-$ZnCl_2$) and 1.0 g (raw CPS), agitation rate of 150 r/min, contact time of 60 min and temperature of 30°C were constant during the experiment)

$CPSAC\text{-}ZnCl_2$ and raw CPS. Moreover, the decrease in percentage removal stopped at 1.00 and 2.00 mm for $CPSAC\text{-}ZnCl_2$ and raw CPS, respectively. The optimum value of grain size for the treatment was 0.08 mm for both adsorbents, which indicates that the finer the adsorbent particle, the faster and higher the removal efficiency. Figure 7 shows that Pb^{2+} and Co^{3+} were removed to the least extent by $CPSAC\text{-}ZnCl_2$ and raw CPS, respectively.

Effect of pH

Effects of changes in pH on removal of metals from mining wastewater by $CPSAC\text{-}ZnCl_2$ adsorbent and raw CPS are shown in Fig. 8. As the pH changes from acidic to alkaline, the removal efficiencies for most of the metals (i.e. Mn^{2+}, Co^{3+}, Fe^{2+}, Pb^{2+} and Cr^{3+}) increased. The optimum pH value for the treatment by both adsorbents ranged between 6.0 and 8.0. Figure 8 shows that Pb^{2+} had the lowest RE. The increase in percentage removal of some metal ions as observed was explained by Ojoawo et al. (2016) as follows: At higher pH, the adsorbent surface is de-protonated and becomes negatively charged; hence, attraction between this surface and the positively charged metal cations occurred.

Effect of temperature

The effects of changes in temperature on metal removal by $CPSAC\text{-}ZnCl_2$ and raw CPS are shown in Fig. 9. Increases in temperature from 30.0 to 70.0°C resulted in a decrease in percentage removal for all the metals remediated by $CPSAC\text{-}ZnCl_2$. Thus, the optimum RE achieved at optimum temperature of 30°C was 72.3, 89.5, 99.9, 98.8 and 99.8, respectively, for Mn^{2+}, Co^{3+}, Fe^{2+}, Pb^{2+} and Cr^{3+}. Mn^{2+} had the lowest RE. However, for raw CPS the RE for all the selected metals increased as the temperature increased from 30.0 to 70.0°C. Optimum RE occurred at 100.0, 92.9, 100.0, 100.0 and 100.0% for Mn^{2+}, Co^{3+}, Fe^{2+}, Pb^{2+} and Cr^{3+}, respectively. The optimum temperature for the treatment was 70.0°C. Co^{3+} had the lowest RE. This result also showed that activation is required for the adsorption process as temperature is a physical means of activation (Adetoro and Ojoawo, 2020a).

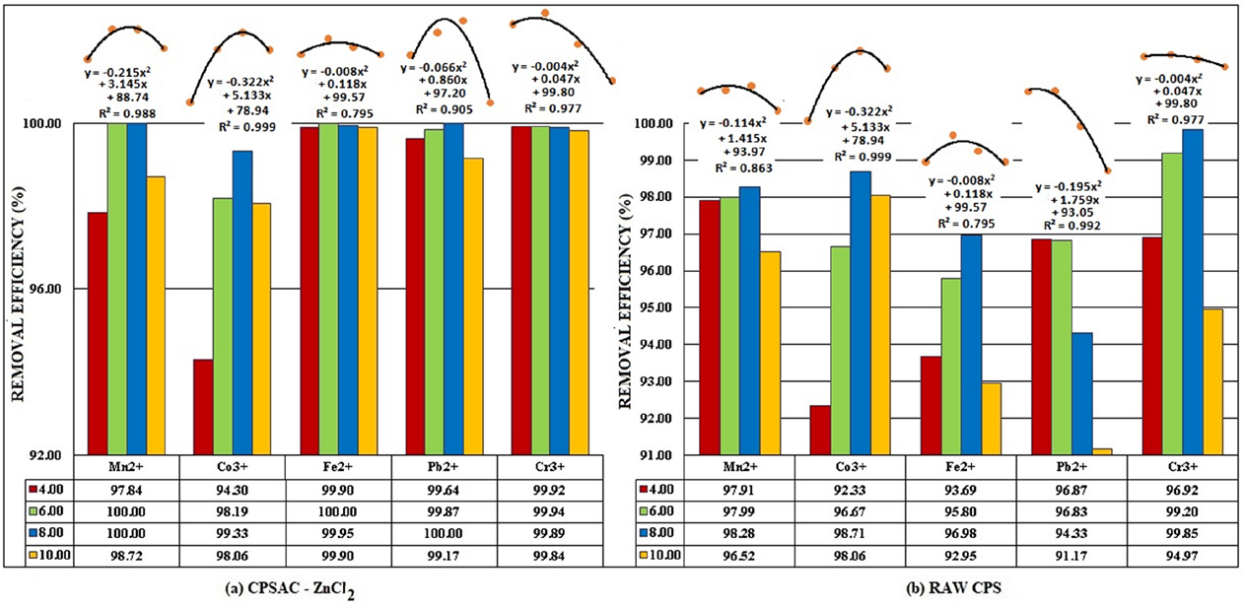

Figure 8. Metal removal efficiency trend with pH (adsorbent dosage of 0.6 g ($CPSAC\text{-}ZnCl_2$) and 1.0 g (raw CPS), agitation rate of 150 r/min, contact time of 60 min, grain size of <2.0 mm and temperature of 30°C were constant during the experiment)

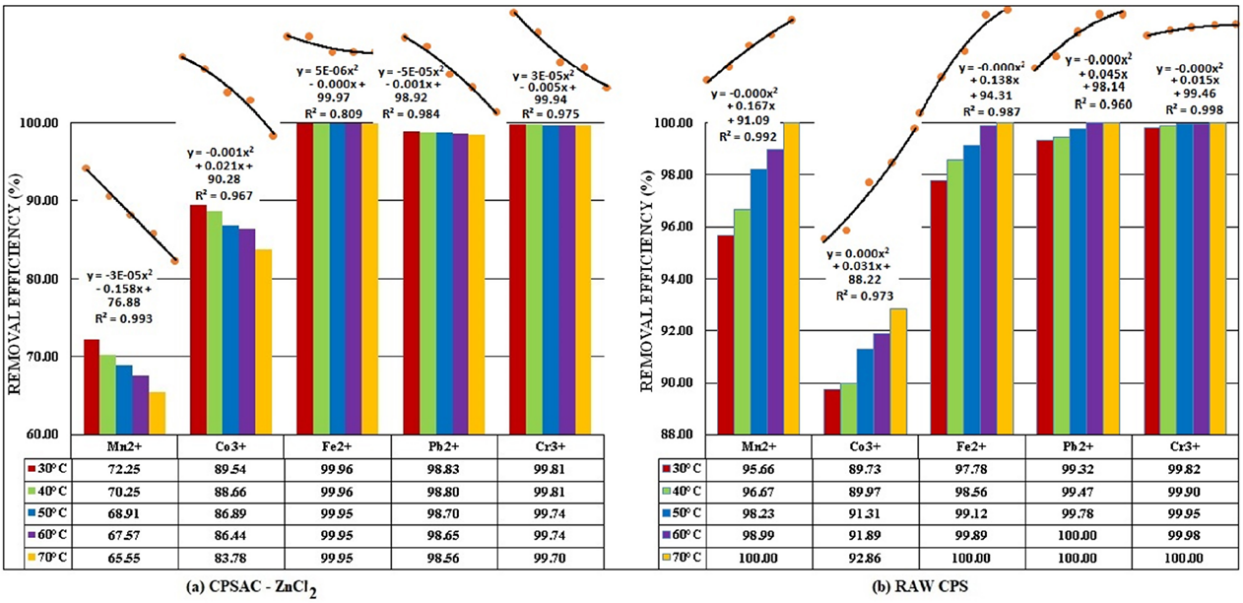

Figure 9. Metal removal efficiency trend with temperature (adsorbent dosage of 0.6 g ($CPSAC\text{-}ZnCl_2$) and 1.0 g (raw CPS), agitation rate of 150 r/min, contact time of 60 min, and grain size of <2.0 mm were constant during the experiment)

Summary: Impact of adsorption parameters

Generally, it was observed that all the adsorption parameters affected the adsorption capacity and removal efficiencies of the raw CPS, but that varying temperature values had the greatest effect: there was an increase in metal removal with increase in temperature. The metals removed also increase as grain size of adsorbent decreased. All the varying dosages of CPSAC-$ZnCl_2$ remediated two metals (i.e. Mn^{2+} and Cr^{3+}) completely while other metal concentrations were greatly reduced. The treatments were affected by contact time of 0.0 to 60.0 min and agitation rate of 50.0 to 150.0 r/min.

The removal efficiencies recorded for all the adsorption parameters proved that activation played an important role(s) in achieving remediation of the selected metals in mining wastewater. Remediated by the raw CPS will reach optimum levels if the biosorbent is physically or chemically activated (especially with $ZnCl_2$).

Results of desorption studies

Table 5 shows the results for desorption efficiency (DE) for the selected metals in mining wastewater treatment using CPSAC-$ZnCl_2$. It can be seen that the DE of the chosen metals was >95% and there was a slow reduction in adsorption of Co^{3+}, Fe^{2+} and Pb^{2+} by CPSAC-$ZnCl_2$ up until the fourth cycle, while adsorption then remained stable up to the sixth cycle. The DE for the other metals remained the same throughout the process. The RE of the adsorbent was also above 95% throughout the process. This indicates that CPSAC–$ZnCl_2$ has a consistently high adsorption capability in removal of the chosen metals from mining wastewater.

Adsorption isotherms

The results of fitting of the Freundlich and Langmuir isotherms to the observed data are presented in Table 6. For the Freundlich isotherm, Fe^{2+} adsorption intensity ($1/n$) is negative for the adsorbent, which indicates irreversible adsorption, $1/n$ of Co^{3+} is greater than 1 (i.e. $1/n > 1$), which indicates non-optimum adsorption; while $1/n$ of Pb^{2+} was between 0 and 1 (i.e. $0 < n < 1$), which indicates optimum adsorption. Only the adsorption of Co^{3+} fitted the Freundlich isotherm with SAE of 5.59 and R^2 of 0.56 when linear regression analysis was applied. For the non-linear regression analysis, all the metal data best fitted the Freundlich isotherm (i.e. close to unity, $R^2 = 1$), in the order of Co^{3+} ($R^2 = 0.99$; SAE = 0.72) > Fe^{2+} ($R^2 = 0.96$; SAE = 4.25) > Pb^{2+} ($R^2 = 0.92$; SAE = 2.59).

The Langmuir isotherm separation factor, R_L, for Co^{3+} was between 0 and 1, which indicated optimum adsorption, while Fe^{2+} and Pb^{2+} have irreversible adsorption as R_L was negative. Co^{3+} and Fe^{2+} data fitted the Langmuir isotherm, with SAE ranging from 3.07 to 86.17 and R^2 from 0.50 to 0.69 using linear regression analysis. All the metals best fitted the Langmuir isotherm, in order of Co^{3+} ($R^2 = 0.99$; SAE = 0.70) > Pb^{2+} ($R^2 = 0.98$; SAE = 4.86) > Fe^{2+} ($R^2 = 0.96$; SAE = 0.03) with non-linear regression analyses.

Adsorption kinetics

The results of fitting the pseudo-second-order and intra-particle diffusion models to the data for metal adsorption by CPSAC-$ZnCl_2$ are presented in Table 7. The observed data closely fitted the pseudo-second-order model, with R^2 generally tending towards unity (i.e. $R^2 = 1$) and SAE of non-linear regression analyses tending towards zero in all cases. The non-linear regression proved to be better for the analysis, due to lower SAE and R^2 values when compared with linear regression analyses, which have large SAE values of 45.911 to 100.920 and R^2 ranging from 0.933 to 0.966.

Moreover, both the q_e (expt.) and q_e (cal.) results were approximately the same for all metals for non-linear regression analyses, which could be due to the rate of adsorption being governed by chemisorption, according to Ojoawo et al. (2016). The determinant factor of the model (i.e. C) varies from 0.57 to 47.18. Fe^{2+} and Co^{3+} have the highest and lowest values of C, respectively.

Adsorption thermodynamics

Adsorption thermodynamics for the selected metals are presented in Table 8. The activation energy (E_a) for the adsorption process ranged between 0 and 518.84 kJ/mol for CPSAC-$ZnCl_2$ and 0 and 134.48 kJ/molfor raw CPS. There was an increase in E_a with increase in temperature for both adsorbents. The E_a for Cu^{2+}, Fe^{2+}, Cd^{2+} and Pb^{2+} with CPSAC-$ZnCl_2$ and for all the metals with raw CPS (except Cu^{2+} and Cr^{3+}) indicate that they underwent physisorption, since their E_a is less than 40.0 kJ/mol.

Table 5. Desorption efficiency of CPSAC-$ZnCl_2$ in the mining wastewater treatment

Desorbing agent	Times	Desorption efficiency (%)							
		Cu^{2+}	Mn^{2+}	Co^{3+}	Fe^{2+}	Zn^{2+}	Cd^{2+}	Pb^{2+}	Cr^{3+}
0.1 M HCl	1	100.0	100.0	99.05	99.6	100.0	100.0	100.0	100.0
	2	100.0	100.0	96.99	99.1	100.0	100.0	99.9	100.0
	3	100.0	100.0	96.08	95.6	100.0	100.0	95.4	100.0
	4	100.0	100.0	96.06	95.5	100.0	100.0	95.4	100.0
	5	100.0	100.0	96.05	95.5	100.0	100.0	95.4	100.0
	6	100.0	100.0	96.05	95.5	100.0	100.0	95.4	100.0

Table 6. Summary of the selected isotherm model parameters for CPSAC-$ZnCl_2$

Isotherm model	Metal	Parameters		Linear regression		Non-linear regression	
Freundlich		$1/n$	K	R^2	SAE	R^2	SAE
	Co^{3+}	3.63	1.54	0.56	5.59	0.99	0.72
	Fe^{2+}	−0.75	2.76	0.47	84.33	0.96	4.25
	Pb^{2+}	0.47	30.61	0.35	22.96	0.92	2.59
Langmuir		R_L					
	Co^{3+}	0.00	36.69	0.69	3.07	0.99	0.70
	Fe^{2+}	0.00	−0.33	0.50	86.17	0.96	0.03
	Pb^{2+}	−0.01	−2.25	0.41	24.28	0.98	4.86

Table 7. Summary of the selected kinetic model parameters for CPSAC-$ZnCl_2$

Kinetic model	Metal	Linear regression				Non-linear regression			
		q_e (expt)	q_e (calc)	R^2	SAE	q_e (expt)	q_e (calc)	R^2	SAE
Pseudo-second-order	Co^{3+}	0.59	0.58	0.96	100.92	0.60	0.60	1.00	0.01
	Fe^{2+}	47.18	47.18	0.93	45.91	47.18	47.18	1.00	0.01
	Pb^{2+}	2.80	2.79	0.97	93.30	2.80	2.80	1.00	0.03
		C	K_{diff}			C	K_{diff}		
Intra-particle diffusion	Co^{3+}	0.61	0.00	0.50	1.05	0.57	0.01	1.00	0.03
	Fe^{2+}	47.18	0.00	0.50	78.65	47.16	0.00	1.00	0.02
	Pb^{2+}	2.79	3×10^{-4}	0.50	4.61	4.022	−0.71	0.97	0.05

Table 8. Adsorption thermodynamic parameters for CPSAC-$ZnCl_2$ and raw CPS

Temperature (°C)	Parameter	CPSAC-$ZnCl_2$								Raw CPS							
		Cu^{2+}	Mn^{2+}	Co^{3+}	Fe^{2+}	Zn^{2+}	Cd^{2+}	Pb^{2+}	Cr^{3+}	Cu^{2+}	Mn^{2+}	Co^{3+}	Fe^{2+}	Zn^{2+}	Cd^{2+}	Pb^{2+}	Cr^{3+}
30	R^2	0.00	0.93	0.88	0.32	0.15	0	0.06	0.82	0.00	0.93	0.88	0.323	0.150	0.00	0.00	0.82
	ΔS	0.00	9.40	11.55	64.51	84.64	0	35.61	45.81	36.46	0.00	16.89	0.00	0.00	0.00	0.00	56.54
	ΔH	0.00	38.34	60.95	14.11	458.33	0	5.71	61.04	38.22	0.00	35.06	0.00	0.00	0.00	0.00	118.80
	ΔG	0.00	−1 621	−5 409	−19 102	−16 489	0	−10 913	−15 756	−6 473	0.00	−6 464	0.00	0.00	0.00	0.00	−20 293
	E_a	0.00	38.34	60.95	14.11	458.33	0	5.71	61.04	38.22	0.00	35.06	0.00	0.00	0.00	0.00	118.80
40	ΔS	0.00	9.40	11.55	64.51	84.64	0	35.61	45.81	36.00	0.00	16.89	0.00	0.00	0.00	0.00	56.54
	ΔH	0.00	39.60	62.96	14.57	473.46	0	5.90	63.06	39.48	0.00	36.22	0.00	0.00	0.00	0.00	122.72
	ΔG	0.00	−1 911	−5 351	−19 732	0.00	0	−11 544	−16 276	−6 581	0.00	−6 122	0.00	0.00	0.00	0.00	−22 646
	E_a	0.00	39.60	62.96	14.57	473.46	0	5.90	63.06	0.00	0.00	36.22	0.00	0.00	0.00	0.00	122.72
50	ΔS	0.00	9.40	11.55	64.51	84.64	0	35.61	45.81	36.46	0.00	16.89	0.00	0.00	0.00	0.00	56.54
	ΔH	0.00	40.87	64.97	15.04	488.59	0	6.09	65.07	40.75	0.00	37.37	0.00	0.00	0.00	0.00	126.64
	ΔG	0.00	−2 137	−5 078	−20 729	−22 708	0	−11 355	−15 948	−6 576	0.00	−5 821	0.00	0.00	0.00	0.00	−20 501
	E_a	0.00	40.87	64.97	15.04	488.59	0	6.09	65.07	40.75	0.00	37.37	0.00	0.00	0.00	0.00	126.64
60	ΔS	0.00	9.40	11.55	64.51	84.64	0	35.61	45.81	36.46	0.00	16.89	0.00	0.00	0.00	0.00	56.54
	ΔH	0.00	42.14	66.98	15.51	503.71	0	6.27	67.09	42.01	0.00	38.53	0.00	0.00	0.00	0.00	130.56
	ΔG	0.00	−2 378	−5128	−20 993	−23 411	0	−11 994	−16 442	−6 565	0.00	−6 001	0.00	0.00	0.00	0.00	−19 738
	E_a	0.00	42.14	66.98	15.51	503.71	0	6.27	67.09	42.01	0.00	38.53	0.00	0.00	0.00	0.00	130.56
70	ΔS	0.00	9.40	11.55	64.51	84.64	0	35.61	45.81	36.46	0.00	16.89	0.00	0.00	0.00	0.00	56.54
	ΔH	0.00	43.40	68.99	15.97	518.84	0	6.46	69.10	43.27	0.00	39.69	0.00	0.00	0.00	0.00	134.48
	ΔG	0.00	−2 729	−4 683	−22 012	−21 558	0	−12 354	−16 581	−6 442	0.00	−6 921	0.00	0.00	0.00	0.00	−21 771
	E_a	0.00	43.40	68.99	15.97	518.84	0	6.46	69.10	43.27	0.00	39.69	0.00	0.00	0.00	0.00	134.48

The remaining metals, for both adsorbents, underwent chemisorption (i.e. $40.0 \leq E_a \leq 800.0$ kJ/mol.) (Bello et al., 2019). The negative and positive values of respective ΔG (negative values) and ΔH (positive values) portrayed the adsorption operations to be favourable, feasible and spontaneous, with weak attraction forces. The ΔS (i.e. positive values) showed an erratic increase in entropy at the solid–solution interface components during the adsorption. The higher adsorption capacity and temperatures were as a result of activation; consequently expansion of the pore size and surface area.

CONCLUSIONS

Activating *Carica papaya* stem with $ZnCl_2$ (CPSAC-$ZnCl_2$) increased the number of metals removed from mining wastewater from two (raw CPS-Zn^{2+} and Cd^{2+}) to five (i.e. Cu^{2+}, Mn^{2+}, Zn^{2+}, Cd^{2+} and Cr^{3+}), while the concentrations of the remaining metals were drastically reduced at optimum conditions of 0.60 g adsorbent dosage, 150.0 r/min agitation rate, 60 min contact time, pH of 7.0 and 30°C temperature. The adsorption processes were positively affected by adsorbent dosage, agitation rate and contact time. Most of the metal adsorption processes were irreversible, while the remaining few best fitted Freundlich and Langmuir isotherm models, pseudo-second-order kinetic model based on non-linear regression analyses and considering SAE and R^2 values. The adsorption processes were favourable, feasible and spontaneous with weak attraction forces. The studied adsorbent (CPSAC-$ZnCl_2$) has a removal efficiency that is above 95.0%, and is thus suitable as a favourable replacement for conventional activated carbon in remediating toxic metals from actual wastewater.

ACKNOWLEDGEMENTS

The authors wish to acknowledge the laboratory assistance rendered by the Department of Civil Engineering, Ladoke Akintola University of Technology, Ogbomoso, Nigeria.

AUTHOR CONTRIBUTIONS

Prof. Samson O Ojoawo: conceptualization, methodology, software, resources, supervision, writing - reviewing and editing.

Dr Ezekiel A Adetoro: data collation, methodology, software, resources, field work, laboratory analysis, formal analysis, writing-original draft preparation, visualization, investigation, validation.

Engr AM Salman: data collation, methodology, software, resources, field work, laboratory analysis, investigation, validation.

CONFLICT OF INTEREST

The authors declare that there are no conflicts of interest regarding the publication of this manuscript. Funding: This research did not receive any specific grant from funding agencies in the public, commercial, or not-for-profit sectors.

REFERENCES

ACHEAMPONG MA and ANSA EDO (2017) Low cost technologies for mining wastewater treatment. *J. Environ. Sci. Eng.* **B** (6) 391–405. https://doi.org/10.17265/2162-5263/2017.08.001

ADETORO EA and OJOAWO SO (2020a) Optimization study of biosorption of toxic metals from mining wastewater using *Azadirachta indica* bark. *Water Sci. Technol.* **82** (5) 887–904. https://doi.org/10.2166/wst.2020.394

ADETORO EA and OJOAWO SO (2020b) Efficiency of *Carica papaya* stem activated with phosphoric acid and sodium hydroxide in mining wastewater treatment. In: *Proceedings of the International Conference on Emerging Trends in Engineering – Civil Engineering Trends and Challenges for Sustainability*, 22–23 December, 2020, Nitte, India. https://doi.org/10.1007/978-981-16-2826-9_6

AGHALARI Z, DAHMS H, SILLANPAA M, JUAN ES and ROBERTO P (2020) Effectiveness of wastewater treatment in removing microbial agents: a systematic review. *Globalization Health.* **16** (13) 1–11. https://doi.org/10.1186/s12992-020-0546-y

ALALWAN HA, KADHOM MA and ALMINSHID AH (2020) Removal of heavy metals from wastewater using agricultural byproducts. *J. Water Suppl. Res. Technol.—Aqua.* **69** (2) 99–112. https://doi.org/10.2166/aqua.2020.133.

AL-FAKIH AA (2015) Biosorption of Ni^{2+} and Cd^{2+} from aqueous solutions using NaOH-treated biomass of *Eupenicillium ludwigii*: Equilibrium and mechanistic studies. *Open J. Appl. Sci.* **5** 376–392. http://doi.org/10.4236/ojapps.2015.57038

AYUB S and KORASGANI FC (2014) Adsorption process for wastewater treatment by using coconut shell. *Res. J. Chem. Sci.* **4** (12) 1–8.

BELLO OS, ADEGOKE KA, FAGBENRO SO and LAMEED OS (2019) Functionalized coconut husks for rhodamine-B dye sequestration. *Appl. Water Sci.* **9** (189) 1–15. https://doi.org/10.1007/s13201-019-1051-4

BISWAS S, BAL M, BEHERA SK, TUSHAR KS and MEIKAP BC (2019) Process optimization study of Zn^{2+} adsorption on biochar-alginate composite adsorbent by response surface methodology (RSM). *Water (MDPI).* **11** (325) 1–15. https://doi.org/10.3390/w11020325

COATES J (2014) *Encyclopedia of Analytical Chemistry: Interpretation of Infrared Spectra (A Practical Approach).* John Wiley & Sons Ltd, Chichester. 10 837 pp.

CZIKKELY M, NEUBAUER E, FEKETE I, YMERI P and FOGARASSY C (2018) Review of heavy metal adsorption processes by several organic matters from wastewaters. *Water (MDPI).* **10** (1377) 1–15. https://doi.org/10.3390/w10101377

EL-MOSELHY KM, AZZEM MA, AMER A and AL-PROL AE (2017) Adsorption of Cu (II) and Cd (II) from aqueous solution by using rice husk adsorbent. *Phys. Chem.: Indian J.* **12** (2) 109–121.

EMENIKE PC, OMOLE DO, NGENE BU and TENEBE IT (2016) Potentiality of agricultural adsorbent for the sequestering of metal ions from wastewater. *Glob. J. Environ. Sci. Manage.* **2** (4) 411–442.

MUSA A, WAN ALWI SR, NGADI N and ABBASZADEH S (2017) Effect of activating agents on the adsorption of ammoniacal nitrogen using activated carbon *papaya* peel. *Chem. Eng. Transact.* **56** 841–846. https://doi.org/10.3303/cet1756141

OJOAWO SO and UDAYAKUMAR G (2016) Remediation and adsorption studies of Pb^{2+} and Cu^{2+} in fresh foundry wastewater using activated charcoal-250. *Adv. Multidisc. Sci. Res.* **2** (3) 67–82.

OJOAWO SO, UDAYAKUMAR G, ADEWALE AA and OGUNOWO AT (2016) Adsorption potentials of *carica papaya* in remediating Pb^{4+} and Cr^{3+} from metal – galvanizing industrial Wastewater. *Int. J. Innovative Trends Eng.* **21** (01) 52–61.

SHALNA T and YOGAMOORTHI A (2015) Preparation and characterization of activated carbon from used tea dust in comparison with commercial activated carbon. *Int. J. Recent Sci. Res.* **6** (2) 2750–2755.

SANUSI KA, UMAR BA and SANI IM (2016) Evaluation of the application of *Carica papaya* seed modified feldspar clay for adsorption of Pb^{2+} and Cu^{2+} in aqueous media: Equilibrium and thermodynamic studies. *J. Environ. Anal. Toxicol.* **6** (2) 1–9.

SMILY JRMB and SUMITHRA PA (2017) Optimization of chromium biosorption by fungal adsorbent, trichoderma sp. BSCR02 and its desorption studies. *Hayati J. Biosci.* **24** (2017) 65–71. https://doi.org/10.1016/j.hjb.2017.08.005

SULAIMAN MS and GARBA MD (2014) Biosorption of Cu(II) ions from aqueous solution using *Azadirachta indica* (neem) leaf powder. *Chem. Process Eng. Res.* **27** 1–11.

SUYONO T, YUSER MA, MUNAF E, AZIZ H, TJONG DH and ZEIN R (2015) Removal of Pb (II) ions by using *papaya* (*carica papaya* l) leaves and petai (parkia speciosa hassk) peels as biosorbent. *J. Chem. Pharm. Res.* **7** (9) 100–106.

UNIOSUN LABORATORY MANUAL – ULM (2017) Laboratory Manual for Students. College of Agriculture, University of Osun, Ejigbo, Nigeria. 78 pp.

WHO (2011) Guidelines for Drinking-Water Quality. World Health Organization, Geneva. 564 pp.